THE UNIVERSITY OF MICHIGAN

COLLEGE OF ENGINEERING
Department of Aeronautical and Astronautical Engineering

Technical Report

INTERACTION EFFECTS OF A JET FLAP ON A 60° DELTA WING AT MACH NUMBER 4, AND COMPARISON WITH TWO-DIMENSIONAL THEORY

James L. Amick Gerard F. Carvalho

ORA Project 03942

under contract with:

DEPARTMENT OF THE NAVY
BUREAU OF NAVAL WEAPONS
CONTRACT NO. NOrd-16595
WASHINGTON, D.C.

through:

APPLIED PHYSICS LABORATORY
THE JOHNS HOPKINS UNIVERSITY
SILVER SPRING, MARYLAND

administered through:

OFFICE OF RESEARCH ADMINISTRATION ANN ARBOR

February 1963

ABSTRACT

Measured normal force increments due to a jet flap issuing perpendicularly from a flat plate wing are presented. Interaction effects caused a magnification of the jet force by a factor of 2.4 to 2.8, when the wing had a turbulent boundary layer. For a laminar boundary layer the jet force magnification ratio varied from 2.5 for the strongest jet tested, to 3.6 for a jet approximately one-tenth as strong. A three-fold change in slot width had very little effect on the interaction.

The experimental results are compared with calculations based on a two-dimensional theory which makes use of empirical separation and base pressure data. The calculated interaction forces are larger than those obtained experimentally, but many of the trends are similar. The interaction is predicted to become increasingly more favorable as Mach number increases. At hypersonic speeds it is indicated that a jet flap wing may be competitive in lifting efficiency with a conventional wing at angle of attack, if operation at large lift coefficients is required.

TABLE OF CONTENTS

LIST OF FIGURES

LIST OF SYMBOLS

a	speed of sound
a_o	stagnation speed of sound of jet
A,B,C,D	functions in Eq. (5)
G	jet impulse function in Eq. (8)
I_s	specific impulse ($= N_\Delta/\dot{m}$)
$I_{s_{vac}}$	specific impulse for discharge into vacuum ($= N_{vac}/\dot{m}$)
L	distance from leading edge to jet
$\dot{m}$	mass flow rate of jet
M	Mach number
M_1	Mach number of flow ahead of separation
N_I	interaction force (normal force due to jet-induced pressure differences outside the jet nozzle)
N_{vac}	theoretical normal force for discharge into vacuum
N_Δ	increment in normal force due to jet, including interaction effects. (Normal force on body in supersonic flow with jet on, minus normal force in supersonic flow with jet off.)
p_1	pressure on surface ahead of separation
p_2	plateau pressure downstream of separation
p_b	base pressure
p_{oj}	jet stagnation pressure
r	local radius of jet
R	radius of forward edge of jet

LIST OF SYMBOLS (Concluded)

Re	Reynolds number based on distance from leading edge to separation point and flow conditions ahead of separation
Re_L	Reynolds number based on distance L and flow conditions ahead of separation
S	distance from separation point to jet
V	velocity
w	exit width of jet slot
w*	throat width of jet slot
w'	equilibrium width of jet after leaving nozzle
β	flow intersection
γ	specific heat ratio of jet gas
δ	separation angle
θ	polar coordinate of curving jet
ρ	mass density
ρ_o	stagnation mass density of jet

INTRODUCTION

A jet issuing from a spanwise slot near the trailing edge of a wing and inclined downward from the chord plane can produce, at subsonic speeds, increases in lift many times larger than the jet momentum force. Such a jet flap can also give substantial lift augmentation at supersonic speeds, as shown by the results of Refs. 1-4, for example.

The tests of Refs. 1 and 2 have shown that the interaction between the jet flap and the main supersonic flow resulted in a total normal force due to the jet which was approximately 2.5 times as large as the direct jet momentum force, for free stream Mach numbers between about 1.5 and 2.5. More recent results at Mach number 6.0 (Ref. 4), tend to confirm this level of interaction, with the important exception that for jets from very narrow slots total forces as high as 10 times the jet momentum force are indicated. The present investigation was undertaken in order to obtain more information about this narrow-jet effect and its possible application to finite-span wings.

The investigation consisted of normal force tests of a tapered jet flap issuing from a slot of variable width, together with a theoretical analysis of two-dimensional jet flap interaction. For the tests a triangular slot planform was chosen, tapering to zero width near each wingtip, in order to minimize tip spillage of the high pressure air in the separation region ahead of the jet. With this arrangement it was hoped to obtain, on a finite-span wing, interaction forces approaching those of a two-dimensional configuration.

THEORETICAL ANALYSIS

Flow Model.—The flow past a two-dimensional jet issuing perpendicularly from a flat surface into a supersonic stream can be idealized according to the model sketched in Fig. 1. The jet issuing from the slot obstructs the flow along the surface causing the boundary layer to separate some distance upstream of the slot. The jet therefore has a region of constant pressure p_2 upstream of it, and another region of constant (lower) pressure p_b downstream of it. Under the influence of this constant pressure difference the jet curves downstream. It is assumed that the jet comes to an equilibrium with the pressure difference after traveling a short distance from the jet exit, and from then on its radius of curvature R is a constant until the flow intersection point is reached.

With this flow model, the interaction force per unit span caused by the jet flap is merely the pressure difference p_2-p_1 times the distance S between the slot and the separation point. This distance is approximately

$$S = R\left(\frac{\cos \beta}{\sin \delta} - 1\right) \tag{1}$$

The jet interaction force is then

$$N_I = (p_2-p_1)R\left(\frac{\cos \beta}{\sin \delta} - 1\right) \tag{2}$$

Before this expression can be evaluated, other relations among the variables must be found. In the following section the jet radius of curvature R will be examined.

Jet Curvature.—Consider a two-dimensional inviscid jet of constant width w' following a circular path under the influence of the transverse pressure difference p_2-p_b. The radial increase in pressure on a fluid element $(rd\theta)(dr)$ must be just sufficient to balance the centrifugal force. Thus

$$(rd\theta)dp = \frac{\rho(rd\theta)(dr)V^2}{r}$$

where r and θ are polar coordinates of the fluid element. For isentropic flow of a perfect gas this equation becomes

$$\frac{dr}{r} = \frac{(\gamma-1)d(p/p_{oj})}{2\gamma(p/p_{oj})\left[(p/p_{oj})^{(\gamma-1)/\gamma} - 1\right]} \tag{3}$$

where γ is the specific heat ratio of the jet gas. Upon integration there results

$$r = R\sqrt{\frac{1-(p_2/p_{oj})^{(\gamma-1)/\gamma}}{1-(p/p_{oj})^{(\gamma-1)/\gamma}}} \tag{4}$$

This result will be used to obtain a relation between the jet radius of curvature R (see Fig. 1) and the mass flow.

The mass flow per unit span is

$$\dot{m} = \int_{R-w'}^{R} \rho V dr = \rho_o a_o \int_{R-w'}^{R} \frac{\rho}{\rho_o}\frac{a}{a_o} M\, dr$$

With the assumption of isentropic flow, and using Eqs. (3) and (4), this becomes,

$$\dot{m} = \rho_o a_o R \frac{\sqrt{(\gamma-1)/2}}{\gamma}\sqrt{1-(p_2/p_{oj})^{(\gamma-1)/\gamma}} \int_{p_b/p_{oj}}^{p_2/p_{oj}} \frac{d(p/p_{oj})}{1-(p/p_{oj})^{(\gamma-1)/\gamma}}$$

where ρ_o and a_o are the stagnation density and speed of sound of the jet gas. The integrand is of the form

$$\left[(1-X^{(\gamma-1)/\gamma})^{-1}\right. = 1 + X^{(\gamma-1)/\gamma} + X^{2(\gamma-1)/\gamma} + X^{3(\gamma-1)/\gamma} + \ldots.$$

Integration of the mass flow equation therefore yields an infinite series. If the radical $\sqrt{1-(p_2/p_{oj})^{(\gamma-1)/\gamma}}$ is expanded and combined with this series, the mass flow equation becomes

$$R = \frac{\dot{m}\, a_o \sqrt{2/(\gamma-1)}}{p_2\left[1 - \frac{p_b}{p_2} + A\left(\frac{p_2}{p_{oj}}\right)^{(\gamma-1)/\gamma} + B\left(\frac{p_2}{p_{oj}}\right)^{2(\gamma-1)/\gamma} + C\left(\frac{p_2}{p_{oj}}\right)^{3(\gamma-1)/\gamma} + \ldots.\right]} \quad (5)$$

where

$$A \equiv \frac{\gamma}{2\gamma-1}\left[1 - \left(\frac{p_b}{p_2}\right)^{(2\gamma-1)/\gamma}\right] - \frac{1}{2}\left(1 - \frac{p_b}{p_2}\right)$$

$$B \equiv \frac{\gamma}{3\gamma-2}\left[1 - \left(\frac{p_b}{p_2}\right)^{(3\gamma-2)/\gamma}\right] - \frac{1}{2}\left(\frac{\gamma}{2\gamma-1}\right)\left[1 - \left(\frac{p_b}{p_2}\right)^{(2\gamma-1)/\gamma}\right] - \frac{1}{8}\left(1 - \frac{p_b}{p_2}\right)$$

$$C \equiv \frac{\gamma}{4\gamma-3}\left[1 - \left(\frac{p_b}{p_2}\right)^{(4\gamma-3)/\gamma}\right] - \frac{1}{2}\left(\frac{\gamma}{3\gamma-2}\right)\left[1 - \left(\frac{p_b}{p_2}\right)^{(3\gamma-2)/\gamma}\right]$$

$$- \frac{1}{8}\left(\frac{\gamma}{2\gamma-1}\right)\left[1 - \left(\frac{p_b}{p_2}\right)^{(2\gamma-1)/\gamma}\right] - \frac{1}{16}\left(1 - \frac{p_b}{p_2}\right)$$

$$D \equiv \frac{\gamma}{5\gamma-4}\left[1 - \left(\frac{p_b}{p_2}\right)^{(5\gamma-4)/\gamma}\right] - \frac{1}{2}\left(\frac{\gamma}{4\gamma-3}\right)\left[1 - \left(\frac{p_b}{p_2}\right)^{(4\gamma-3)/\gamma}\right] - \frac{1}{8}\left(\frac{\gamma}{3\gamma-2}\right)\left[1 -\right.$$

$$\left.\left(\frac{p_b}{p_2}\right)^{(3\gamma-2)/\gamma}\right] - \frac{1}{16}\left(\frac{\gamma}{2\gamma-1}\right)\left[1 - \left(\frac{p_b}{p_2}\right)^{(2\gamma-1)/\gamma}\right] - \frac{5}{128}\left(1 - \frac{p_b}{p_2}\right)$$

The infinite series in the denominator of Eq. (5) converges rapidly so that

only a few terms need be used. Values of the coefficients for typical values of γ and p_b/p_2 are listed below:

γ	p_b/p_2	A	B	C	D
1.4	0	.2778	.1225	.0606	.0302
1.4	.1	.2875	.1380	.0729	.0392
1.2	0	.3571	.1964	.1220	.0803
1.2	.1	.3487	.2033	.1318	.0899

The interaction force is obtained by substituting (5) into (2)

$$N_I = \frac{m\, a_o \sqrt{2/(\gamma-1)} \left(1 - \frac{p_1}{p_2}\right)\left(\frac{\cos\beta}{\sin\delta} - 1\right)}{1 - \frac{p_b}{p_2} + A\left(\frac{p_2}{p_{oj}}\right)^{(\gamma-1)/\gamma} + B\left(\frac{p_2}{p_{oj}}\right)^{2(\gamma-1)/\gamma} + \cdots} \tag{6}$$

The quantities $(1- p_1/p_2)$, $\cos\beta$, and $\sin\delta$ depend on the boundary layer separation and intersection characteristics. The determination of these quantities will be treated later for both laminar and turbulent boundary layers, but first some general formulas for specific impulse will be obtained.

Specific Impulse.—The specific impulse of the total force due to the jet is

$$I_s = \frac{N_\Delta}{\dot{m}} = \frac{N_{vac}}{\dot{m}} + \frac{N_I}{\dot{m}} - \frac{p_1 w}{\dot{m}} \tag{7}$$

where N_{vac} is the force of the jet exhausting into a vacuum, and w is the exit width of the jet slot. The first term on the right of Eq. (7) is the vacuum specific impulse which may be written

$$I_{s_{vac}} = \frac{N_{vac}}{\dot{m}} = \frac{2}{\gamma}\sqrt{\frac{\gamma+1}{2}}\; G\, a_o \tag{8}$$

where G is a complicated function of the jet gas specific heat ratio and the nozzle geometry. The value of G ranges from unity for a sonic nozzle to $\gamma/\sqrt{\gamma^2-1}$ for an ideal nozzle with exit Mach number of infinity.

The last term in (7) can be rewritten using the equation

$$\dot{m} = \rho_o a_o w^* \left[2/(\gamma+1)\right]^{(\gamma+1)/2(\gamma-1)} \tag{9}$$

$$\frac{p_1 w}{\dot{m}} = \frac{p_1}{p_{oj}} \frac{w}{w^*} \frac{a_o}{\gamma} \left(\frac{\gamma+1}{2}\right)^{(\gamma+1)/2(\gamma-1)} \tag{10}$$

By substitution of Eqs. (6), (8), and (10) into Eq. (7), the specific impulse equation becomes

$$I_s = \frac{2}{\gamma}\sqrt{\frac{\gamma+1}{2}}\, G\, a_o - \frac{p_1}{p_{oj}} \frac{w}{w^*} \frac{a_o}{\gamma} \left(\frac{\gamma+1}{2}\right)^{(\gamma+1)/2(\gamma-1)} + \frac{a_o\sqrt{2/(\gamma-1)}\,(1-p_1/p_2)\left(\frac{\cos\beta}{\sin\delta} - 1\right)}{1 - \frac{p_b}{p_2} + A\left(\frac{p_2}{p_{oj}}\right)^{(\gamma-1)/\gamma} + B\left(\frac{p_2}{p_{oj}}\right)^{2(\gamma-1)/\gamma} + \cdots} \tag{11}$$

The ratio of the specific impulse of the jet to that in a vacuum is

$$\frac{I_s}{I_{s_{vac}}} = 1 - \frac{p_1}{p_{oj}} \frac{w}{w^*} \frac{1}{2G} \left(\frac{\gamma+1}{2}\right)^{1/(\gamma-1)} + \frac{\gamma}{\sqrt{\gamma^2-1}} \frac{(1-p_1/p_2)\left(\frac{\cos\beta}{\sin\delta} - 1\right)}{G\left[1 - \frac{p_b}{p_2} + A\left(\frac{p_2}{p_{oj}}\right)^{(\gamma-1)/\gamma} + B\left(\frac{p_2}{p_{oj}}\right)^{2(\gamma-1)/\gamma} + \cdots\right]} \tag{12}$$

This specific impulse ratio may also be thought of as a magnification factor, representing the normal force increment due to the jet (including interaction effects) as a multiple of the normal force of a jet of the same gas discharg-

ing into vacuum thru a geometrically similar nozzle at the same mass flow rate.

Further evaluation of the interaction force or magnification factor requires consideration of the boundary layer separation and intersection characteristics. These characteristics are treated separately for laminar and turbulent boundary layers in the next sections.

Laminar Boundary Layer.--Separation of a laminar boundary layer is a function of both Reynolds number and Mach number as given by the semi-empirical equation (Ref. 5).

$$\frac{p_2}{p_1} = 1 + 1.27\sqrt{\frac{M_1^3}{\sqrt{Re}}}$$

$$= 1 + 1.27\left(\frac{L}{L-S}\right)^{1/4}\sqrt{\frac{M_1^3}{\sqrt{Re_L}}} \qquad (13)$$

where Re_L is the Reynolds number based on distance from the leading edge to the slot and flow conditions at M_1. This equation can be rearranged to give

$$\frac{S}{L} = 1 - \frac{2.60}{(p_2/p_1-1)^4}\left(\frac{M_1^3}{\sqrt{Re_L}}\right)^2 \qquad (14)$$

Another expression for S/L, obtained from (1), (5), and (9), is

$$\frac{S}{L} = \frac{p_{oj}}{p_2}\frac{w^*}{L}\left(\frac{2}{\gamma+1}\right)^{1/(\gamma-1)}\frac{2\gamma}{\sqrt{\gamma^2-1}}\frac{\left(\frac{\cos\beta}{\sin\delta}-1\right)}{\left[1-\frac{p_b}{p_2}+A\left(\frac{p_2}{p_{oj}}\right)^{(\gamma-1)/\gamma}+B\left(\frac{p_2}{p_{oj}}\right)^{2(\gamma-1)/\gamma}+\cdots\right]} \qquad (15)$$

By combining (14) and (15) there results

$$\frac{p_2}{p_{oj}} = \frac{\frac{w^*}{L}\left(\frac{2}{\gamma+1}\right)^{1/(\gamma-1)}\frac{2\gamma}{\sqrt{\gamma^2-1}}\left(\frac{\cos\beta}{\sin\delta}-1\right)}{\left[1-\frac{2.60}{\left(\frac{p_2}{p_1}-1\right)^4}\frac{M_1^6}{Re_L}\right]\left[1-\frac{p_b}{p_2}+A\left(\frac{p_2}{p_{oj}}\right)^{(\gamma-1)/\gamma}+B\left(\frac{p_2}{p_{oj}}\right)^{2(\gamma-1)/\gamma}+\cdots\right]} \qquad (16)$$

The infinite series in the above equation is a weak function of p_2/p_{oj}. Consequently, the equation can be easily solved by iteration. For a given value of p_2/p_1 a trial value of p_2/p_{oj} is chosen. The equation is then used to compute a more accurate p_2/p_{oj}. (The value of δ to be used in this equation is obtained from p_2/p_1 by means of the oblique shock relations.)

The flow intersection angle β must be known in order to use Eq. (16). This angle can be estimated from base pressure data, since the flow near the flow intersection point is basically similar to that behind a blunt base.

At the flow intersection point two superonsic streams (the main flow and the jet) come together and both undergo compressive turns. Both streams are bounded by shear layers, the low-speed portions of which are unable to negotiate the adverse pressure gradient at the flow intersection point. These low-speed layers are therefore turned back into the separated flow region. The flow intersection angle β adjusts itself so that this reversed mass flow is equal to the mass flow entrained by the two shear layers.

This flow mechanism is very similar to that behind a blunt-based body. It therefore seems appropriate to use, for the jet flap, flow intersection angles calculated from base pressure data.

For boundary layers which are laminar at separation, the base pressure data of Van Hise (Ref. 6) at Mach numbers between 2 and 3 indicate flow intersection angles varying from 12° to 45°, depending on the location of the transition point with respect to the separation point. The calculations to be presented later are therefore simply made for several arbitrary values of β.

Turbulent Boundary Layer.—Separation of a turbulent boundary layer is only slightly dependent on Reynolds number. According to the analysis of Chapman, Kuehn, and Larson (Ref. 7), the plateau pressure rise (or first peak pressure rise) should be proportional to the square root of the local skin friction coefficient, which in turn is proportional to the inverse fifth root of Reynolds number, for an incompressible 1/7-power velocity profile. This variation with Reynolds number agrees with some of their data, although in several cases there appears to be no Reynolds number effect, as was also found by Love (Ref. 8).

The Mach number dependence of the plateau pressure rise has been investigated experimentally by Love (Ref. 8) and by Sterrett and Emery (Ref. 9). Their data, together with that of Chapman, Kuehn, and Larson, can be roughly approximate by

$$\frac{p_2}{p_1} = 1 + 2.6 \frac{\sqrt{M_1^2-1}}{(Re)^{1/10}} \tag{17}$$

as shown in Fig. 2. Combining (17) with (15) yields

$$\frac{p_2}{p_{oj}} = \frac{\frac{w^*}{L}\left(\frac{2}{\gamma+1}\right)^{1/(\gamma-1)} \frac{2\gamma}{\sqrt{\gamma^2-1}} \left(\frac{\cos\beta}{\sin\delta} - 1\right)}{\left[1 - \frac{14{,}100\,(M_1^2-1)^5}{\left(\frac{p_2}{p_1} - 1\right)^{10} Re_L}\right]\left[1 - \frac{p_b}{p_2} + A\left(\frac{p_2}{p_{oj}}\right)^{(\gamma-1)/\gamma} + B\left(\frac{p_2}{p_{oj}}\right)^{2(\gamma-1)/\gamma} + \cdots\right]} \tag{18}$$

The flow intersection angle β for turbulent boundary layers can be estimated from the base pressure data of Gadd, Holder, and Regan (Ref. 10). The flow intersection angle calculated from their data reaches a maximum of 39.3° at a Mach number M_2 of about 4.0, and remains greater than 35° for Mach numbers between 2.75 and 6.0. The value of 38° is therefore used in the following

calculations.

Calculated Results.—Numerical calculations have been made, utilizing the methods developed above, in order to show how the specific impulse ratio is affected by various parameters. Typical results are shown in Figs. 3-8. With a turbulent boundary layer the specific impulse ratio is seen (Figs. 3-7) to be relatively insensitive to the jet force-to-aerodynamic force ratio (as represented by the parameter $p_{oj}\ w^*/p_1\ L$). For laminar boundary layers a decrease in specific impulse ratio with increasing jet force ratio is usually indicated.

The choice of flow intersection angle for laminar separation has a fairly strong effect on specific impulse ratio, as shown in Fig. 3. For pure laminar separation a flow intersection angle in the neighborhood of 10° would be expected. On the other hand, if transition occurs soon after separation the flow intersection angle may approach 50°. It is believed that the 50° flow intersection angle is more representative of jet-flap interactions at moderate Reynolds numbers, since the unsteady nature of the jet would tend to promote early transition in the separated shear layer. Accordingly, all the remaining calculations for laminar separation assume a flow intersection angle of 50°.

The base pressure assumed in the calculations is shown in Fig. 4 to have only a small effect on the specific impulse ratio. Zero base pressure is therefore used in all the other calculations.

The effect of the jet slot width is presented in Fig. 5. Decreasing the slot width is shown to give higher specific impulse values, but the effect is rather small for slot widths of the order of 0.1% of the chord length or less.

The jet gas specific heat ratio also has only a relatively minor effect on jet flap interaction, as shown in Fig. 6.

Reynolds number effects are presented in Fig. 7. It is seen that changes in Reynolds number have little effect on jet flap interaction as long as the boundary layer is laminar at separation. For a turbulent boundary layer, however, large changes in Reynolds number can produce large specific impulse changes. In the limit of infinite Reynolds number the only difference between the results for laminar and for turbulent boundary layers is that due to the different flow intersection angles.

Most of the calculated results show a maximum value of specific impulse ratio at some value of jet force parameter. The variation of such maximum specific impulse values with Mach number is presented in Fig. 8. For both laminar and turbulent boundary layers a considerable increase of specific impulse ratio with Mach number is indicated.

The calculated lifting efficiency of a jet-flap wing is compared in Fig. 9 with the lifting efficiency calculated by the shock-expansion method for a flat-plate wing at angle of attack. The two lifting efficiency parameters used in this plot (lift-drag ratio for the flat plate at angle of attack and specific impulse ratio for the wing with jet flap) are directly comparable measures of the lift produced for a given fuel consumption rate chargeable to the lifting device, if the following assumptions are satisfied:

(1) The jet flap produces no change in drag.

(2) The specific impulse of the propulsion system under its operating conditions (thrust developed per unit fuel consumption rate) is equal to the

specific impulse of the jet flap nozzle discharging into a vacuum.

(3) The zero-lift drag of the flat plate wing is equal to that of the jet flap wing, and is excluded from the lift-drag ratio.

The lifting efficiency comparison of Fig. 9 indicates that at hypersonic speeds a jet-flap wing may be competitive in efficiency with a wing at angle of attack, if operation at large lift coefficients is required. Thus, a jet-flap wing might be used to advantage on a hypersonic vehicle requiring extreme maneuverability.

EXPERIMENT

Equipment.—The jet flap force tests were conducted in The University of Michigan 8 x 13 in. vacuum blowdown wind tunnel. The test Mach number was $M = 3.95$, the Reynolds number was approximately $.13 \times 10^6$/in., and the tunnel stagnation pressure and temperature were atmospheric.

The model tested was a 60° delta flat plate (Fig. 10). This model had a tapered slot located very close to the base of the model. The leading edge of the slot was straight, while the trailing edge was formed by a flexible plate so constructed that the slot was triangular, with the maximum width of the slot located on the model center line. With the flexible plate construction, the maximum width of the slot could be varied without altering the basic shape or span of the slot.

The principal quantities measured during the tests were the normal force increment due to the jet, the line of action of this force increment, and the mass flow rate of the jet. The force increment and its line of action were obtained by turning the jet off during a wind tunnel run and observing the changes in bending moment on the cantilever beam supporting the model. The cantilever beam, which was tubular and supplied air to the jet, was instrumented with four strain gage bridges.

The strains induced in the beam by the normal forces on the model were amplified and recorded by a commercial oscillograph. The strain gage bridges were located on the beam in groups of two; two of the bridges were located in such a manner that they were always very close to the center of pressure on

the model, while the other two bridges were located approximately four inches downstream of the center of pressure.

The jet mass flow was measured with a standard ASME sharp-edged orifice meter. Other data obtained during the tests consisted of tunnel stagnation pressure and temperature, jet stagnation pressure, schlieren pictures, and china clay patterns of the boundary layer separation line.

Analyses were made of the force and mass flow measuring systems to determine the accuracy of the results obtained. The results of the analyses indicated that the mass flows measured were accurate within ± 1%, and that the forces were accurate within ± 3% for the smallest forces recorded. The accuracy of the force measuring system improved with increasing force so that the largest forces measured were accurate to within ± 2%.

Experimental Results.—The main results of the jet flap tests are presented in Fig. 11 as specific impulse ratios, i.e., the normal force increment due to the jet (including interaction effects) divided by the theoretical normal force of a jet of the same gas discharging into vacuum thru a geometrically similar nozzle at the same mass flow rate. On the same plot are shown theoretical curves calculated by the two-dimensional theory.

Some qualitative agreement between two-dimensional theory and the finite-span experiments can be seen in Fig. 11. Both theoretical and experimental results show that the interaction force is greater than the jet force in a vacuum, in the range of jet forces tested. Higher values of specific impulse ratio are obtained with laminar than with turbulent boundary layers, and the rate of decrease of this ratio with increasing jet force-to-aerodynamic force

ratio is greater for laminar than for turbulent boundary layers. The effect of a threefold change in the width of the slot from which the jet issues is small.

The values of specific impulse ratio shown in Fig. 11 for the jet flap are within the range of values found in Ref. 11 for a jet issuing from a circular orifice in a flat plate. For the circular jet the rate of decrease of specific impulse with increasing jet force (which rate was independent of boundary layer condition) was greater than the rate of decrease for the jet flap with turbulent boundary layer but less than for the jet flap with laminar boundary layer.

The measured location of the line of action of the increment in normal force due to the jet is plotted in Fig. 12. (In calculating these center of pressure locations from the measured sting bending moments the effect of any change in drag that may be caused by the jet was neglected.) The laminar data show a progressive forward movement of the center of pressure with increasing jet force ratio, in qualitative agreement with the forward movement of the separation point predicted by theory. For the turbulent data there is only a slight indication of such a trend.

Typical schlieren pictures are shown in Fig. 13. These pictures were taken with an exposure time of about 1/50 sec, so that they show only the average positions of the shock waves, which are probably fluctuating, as found in other jet interaction investigations. A schlieren picture of the flow past a triangular spoiler is also included. The spoiler had a 5-in. span and tapered from a .090-in. height at mid span to zero height near each wing tip.

The forward movement of separation with increasing jet force ratio is evident in the schlieren pictures with laminar boundary layers (pictures (a) thru (d) of Fig. 13). The turbulent boundary layer pictures ((e) thru (g)) show much less movement of the separation point.

CONCLUSION

From the present theoretical and experimental investigation of wings with jet flaps in a Mach number 4.0 free stream it is concluded that:

1. Aerodynamic interaction ahead of a jet flap results in a total normal-force increment due to the jet which is approximately 2 to 4 times as large as the jet force in a vacuum, over a wide range of conditions. This force magnification due to interaction of a jet flap is similar in magnitude to that of a circular jet issuing from a flat plate.

2. The width of the slot producing the jet flap has little influence on the force magnification for a fixed value of the jet force-to-aerodynamic force parameter.

3. A wing with jet flap may be competitive in lifting efficiency with a plain wing at angle of attack, for large lift coefficients at hypersonic speeds.

REFERENCES

1. Poisson-Quinton, Ph. and Jousserandot, P., Influence Du Soufflage An Voisinage Du Bord De Fuite Sur Les Caracteristiques Aerodynamiques D'une Aile Aux Grande Vitesses, IX eme Congres International re Mechanique Appliquee, Bruxelles, September 1956.

2. Poisson-Quinton, Ph. and Lepage, L., "French Research on Control of Boundary Layer and Circulation," Boundary Layer and Flow Control, Vol. I, edited by G. V. Lachmann, Pergamon Press, 1961.

3. Schult, E., Free-Flight Investigation at Mach Numbers Between 0.5 and 1.7 of the Zero-Lift Rolling Effectiveness and Drag of Various Surface, Spoiler and Jet Controls on an 80° Delta-Wing Missile, NASA TN D-205, February 1960.

4. Romeo, D. J. and Sterrett, J. R., Aerodynamic Interaction Effects Ahead of a Sonic Jet Exhausting Perpendicularly from a Flat Plate into a Mach Number 6 Free Stream, NASA TN D-743, April 1961.

5. Amick, J. L., A Semiempirical Relation for Laminar Separation, Journal of the Aero/Space Sciences, Vol. 26, No. 9, p. 603, September 1959.

6. Van Hise, V., Investigation of Variation in Base Pressure over the Reynolds Number Range in Which Wake Transition Occurs for Two-Dimensional Bodies at Mach Numbers from 1.95 to 2.92, NASA TN D-167, November 1959.

7. Chapman, D. R., Kuehn, D. M., and Larson, H.K., Investigation of Separated Flows in Supersonic and Subsonic Streams with Emphasis on the Effect of Transition, NACA Rept. 1356, 1958.

8. Love, E. S., Pressure Rise Associated with Shock-Induced Boundary-Layer Separation, NACA TN 3601, December 1955.

9. Sterrett, J. R. and Emery, J. C., Extension of Boundary-Layer-Separation Criteria to a Mach Number of 6.5 by Utilizing Flat Plates with Forward-Facing Steps, NASA TN D-618, December 1960.

10. Gadd, G. E., Holder, D. W., and Regan, J. D., Base Pressures in Supersonic Flow, Aeronautical Research Council, C.P. No. 271, 1956.

11. Amick, J. L. and Hays, P. B., Interaction Effects of Side Jets Issuing from Flat Plates and Cylinders Alined with a Supersonic Stream, WADD TR 60-329, Wright Air Development Division, June 1960.

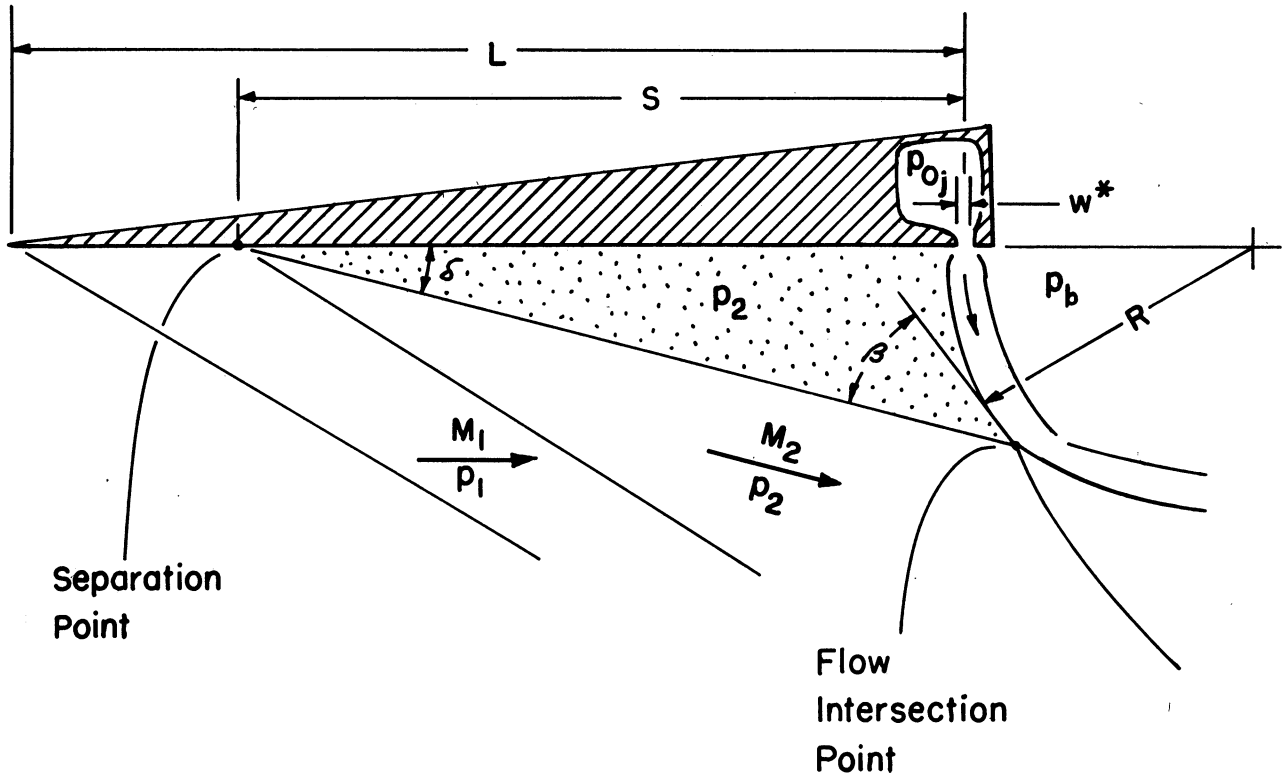

Fig. 1. Flow model for two-dimensional jet-flap interaction.

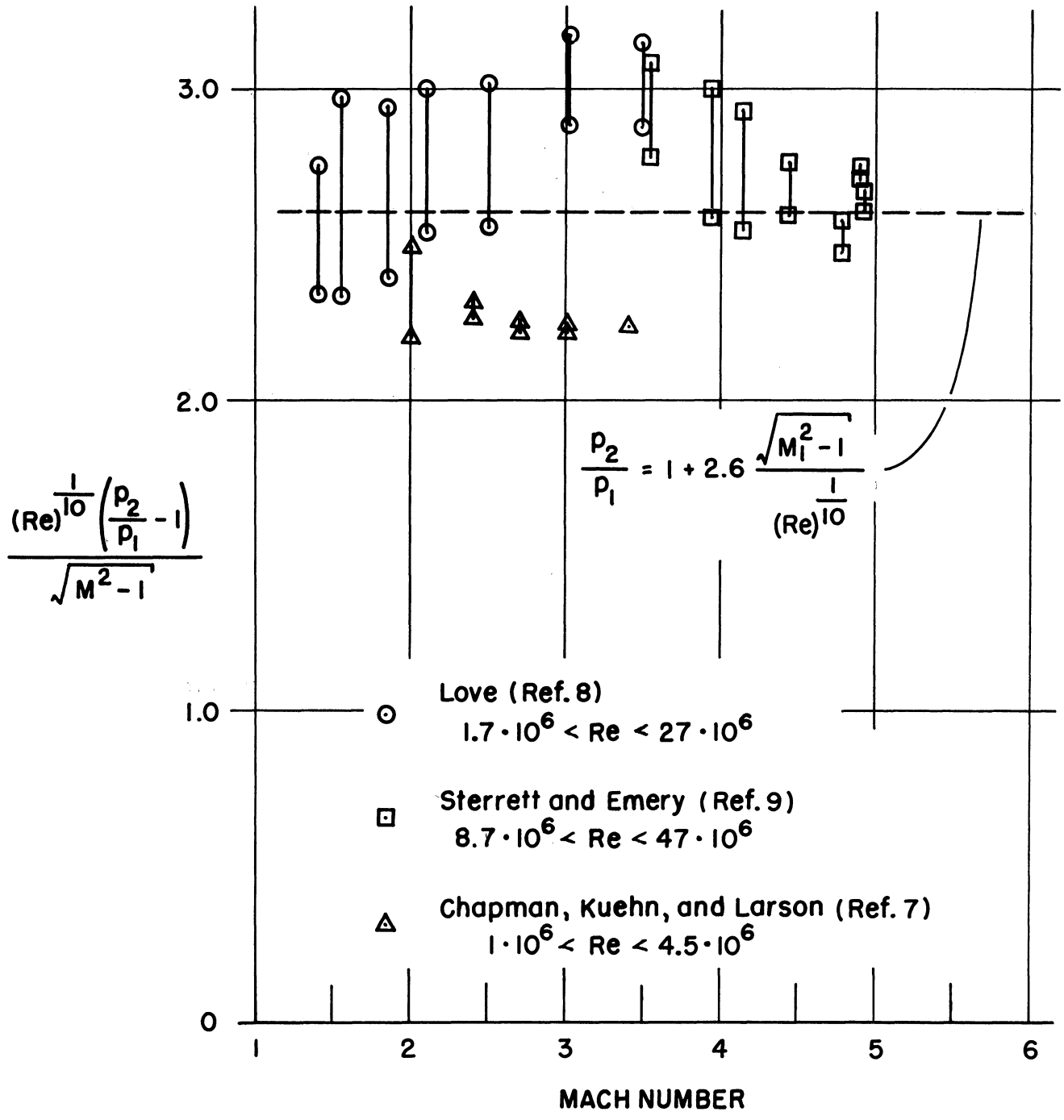

Fig. 2. Correlation of data on plateau pressure rise for turbulent separation.

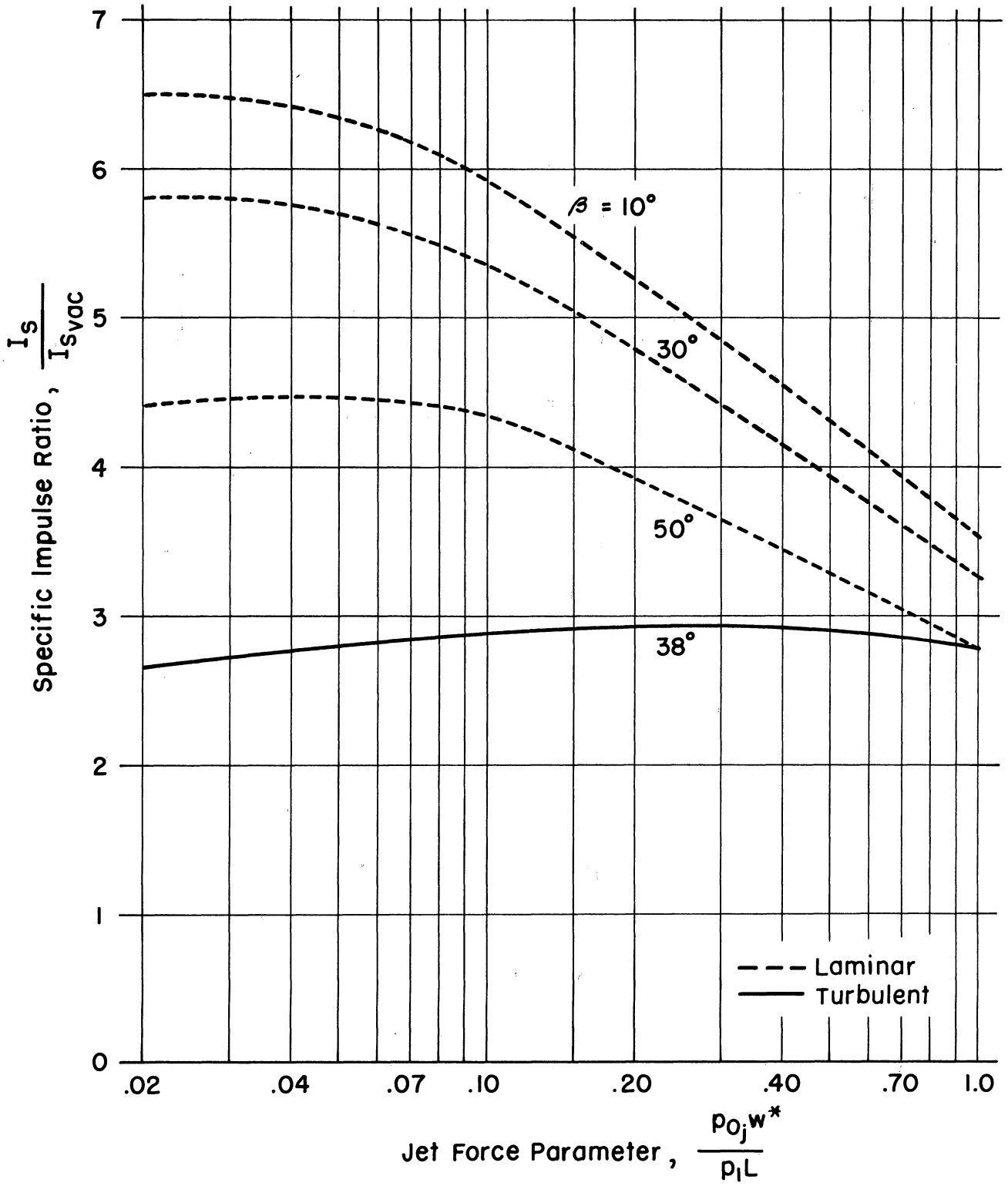

Fig. 3. Calculated specific impulse magnification due to interaction ahead of a two-dimensional jet flap, for laminar and turbulent separation with various flow intersection angles. $M_1 = 4.0$, $Re_L = 500{,}000$, $w^*/L = .001$, $p_b/p_2 = 0$, sonic jet nozzle.

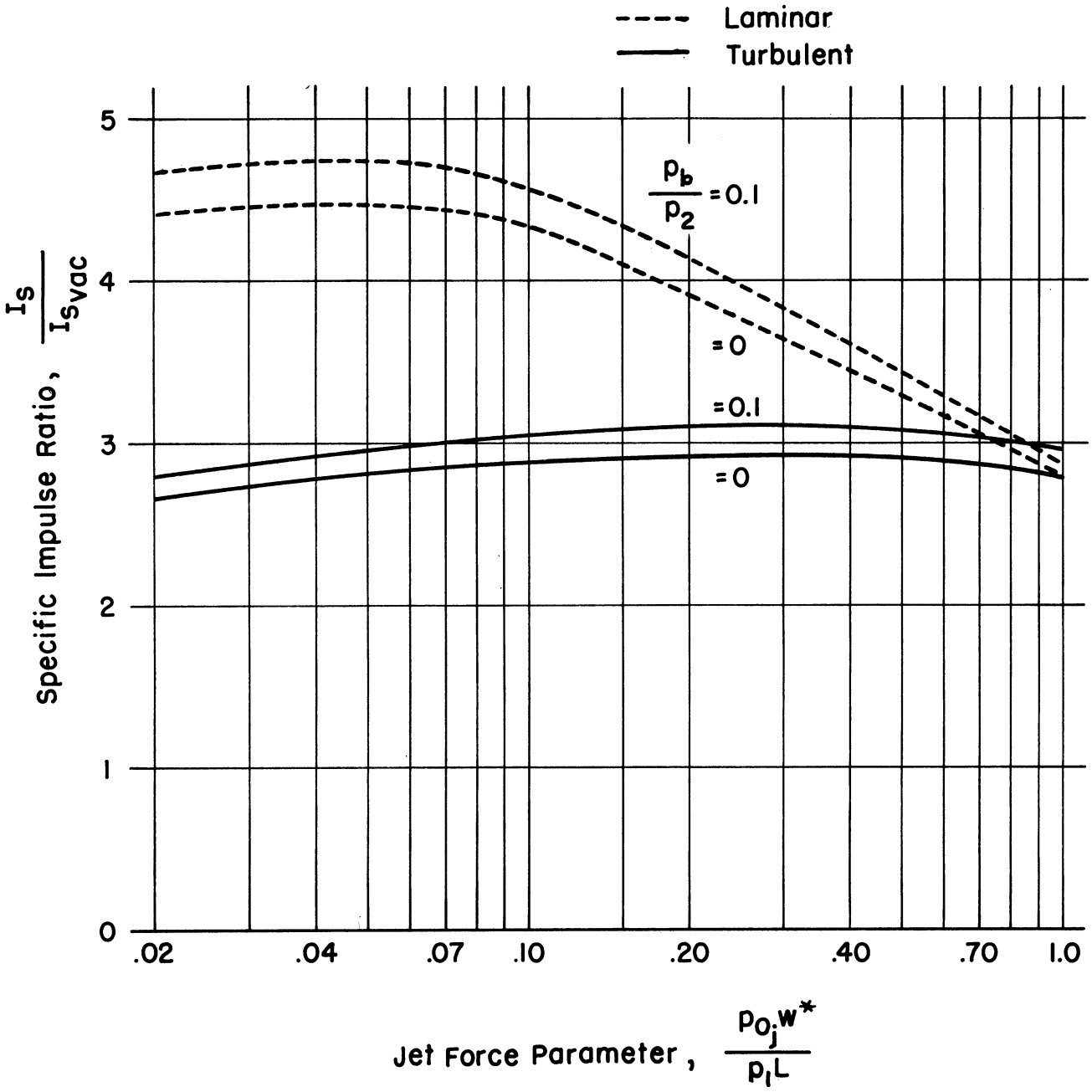

Fig. 4. Effect of base pressure assumption on calculated interaction of a two-dimensional jet flap.

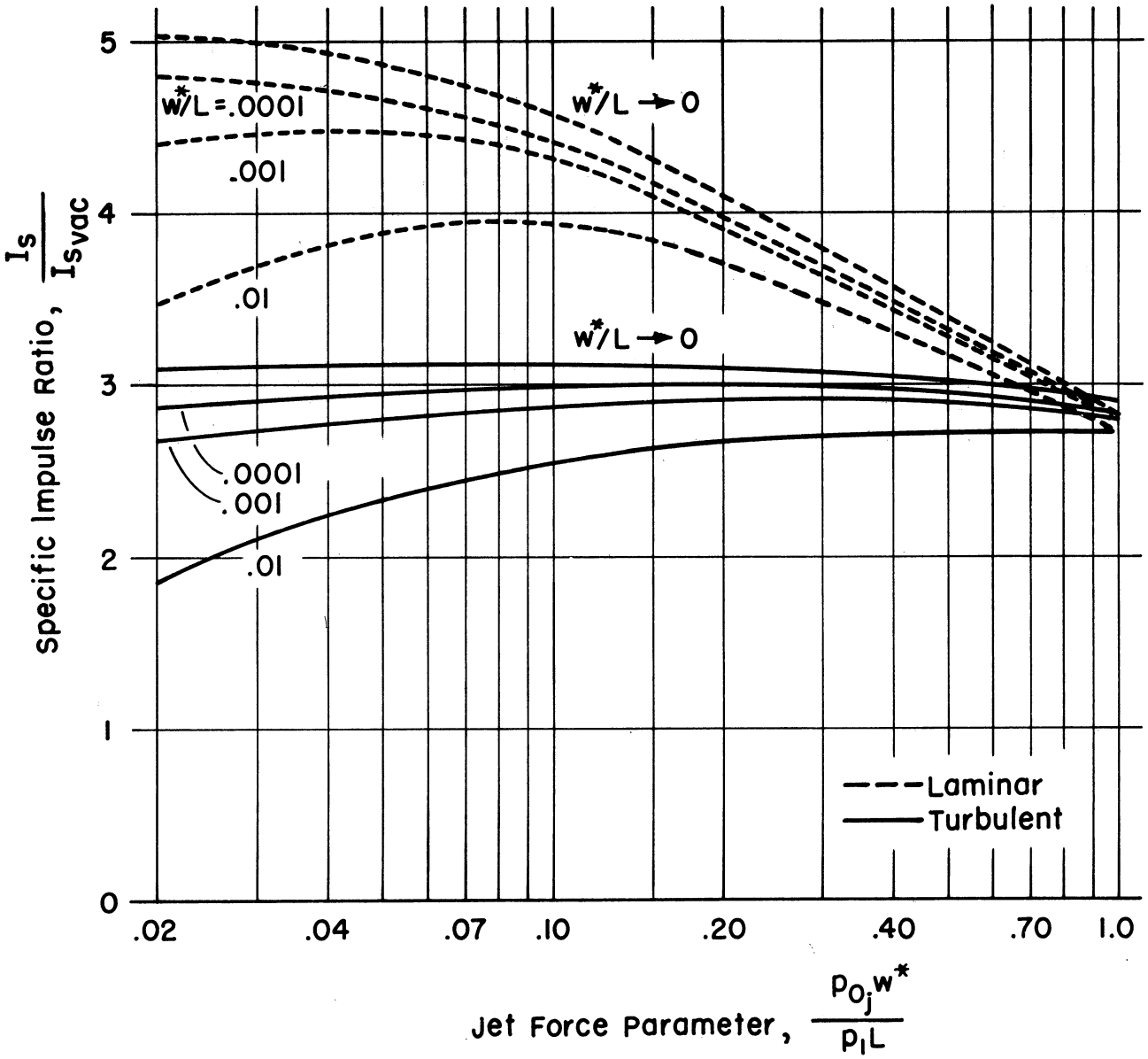

Fig. 5. Effect of jet slot width on calculated interaction of a two-dimensional jet flap.

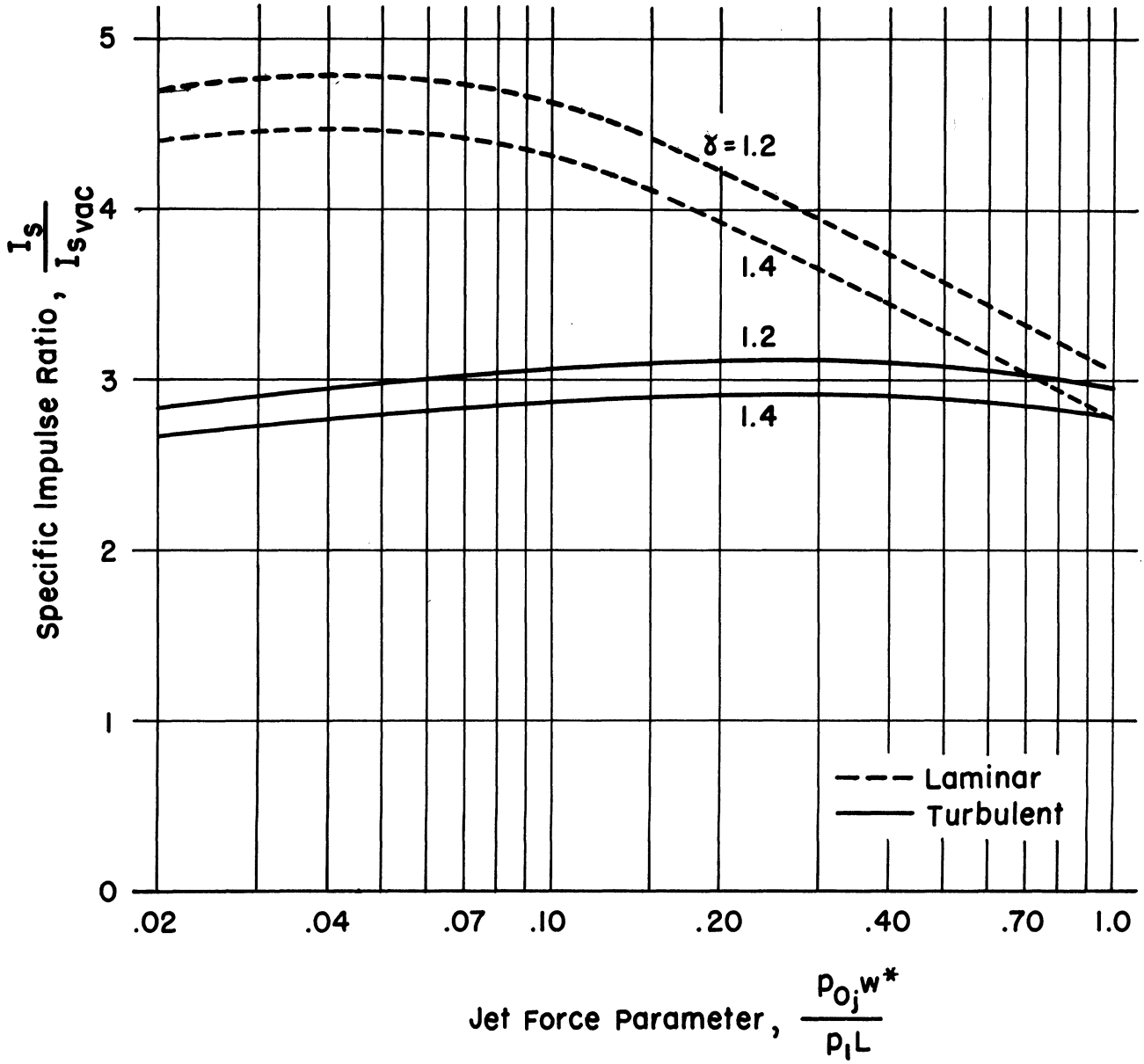

Fig. 6. Effect of jet gas specific heat ratio on calculated interaction of a two-dimensional jet flap.

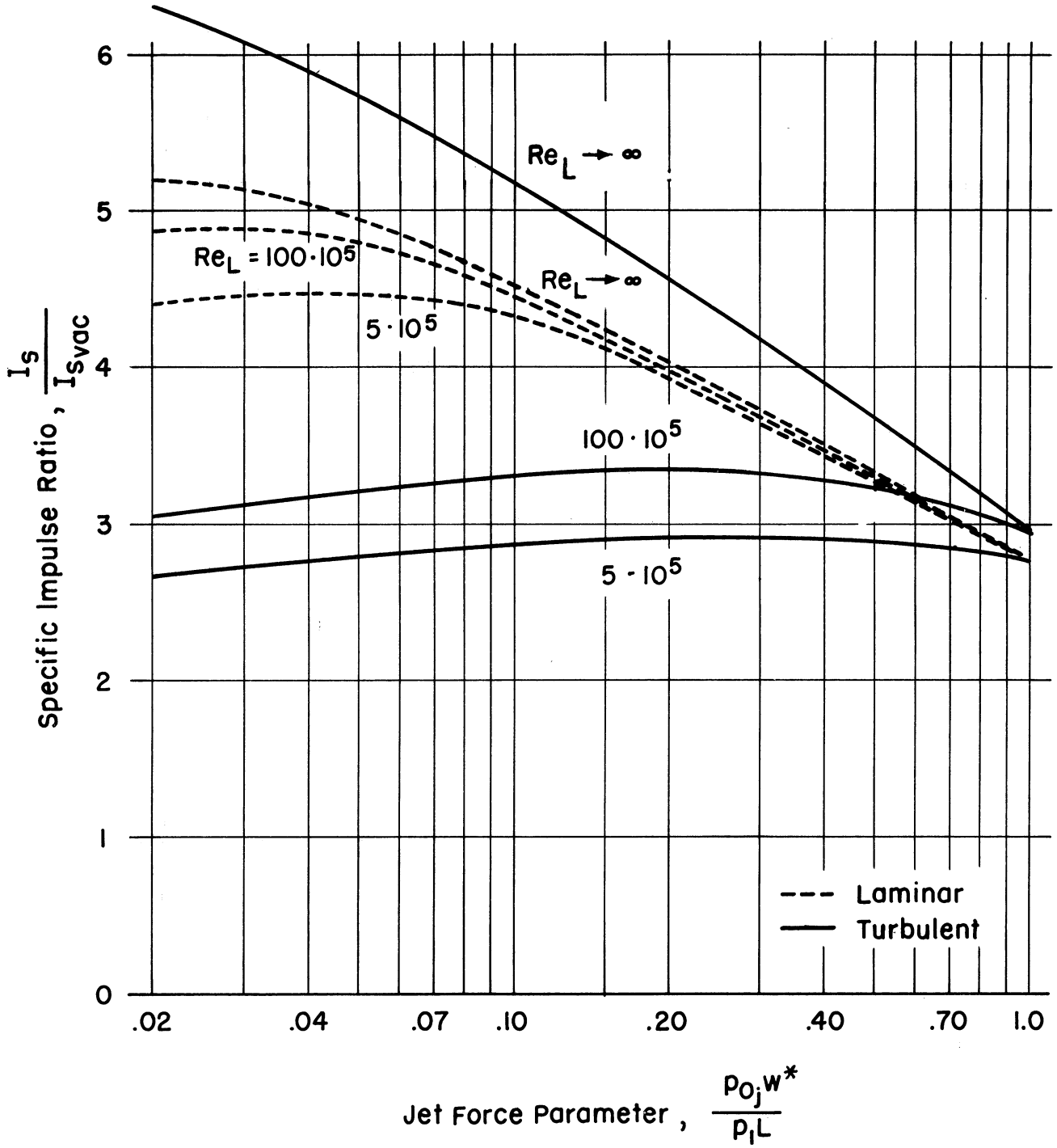

Fig. 7. Effect of Reynolds number on calculated interaction of a two-dimensional jet flap.

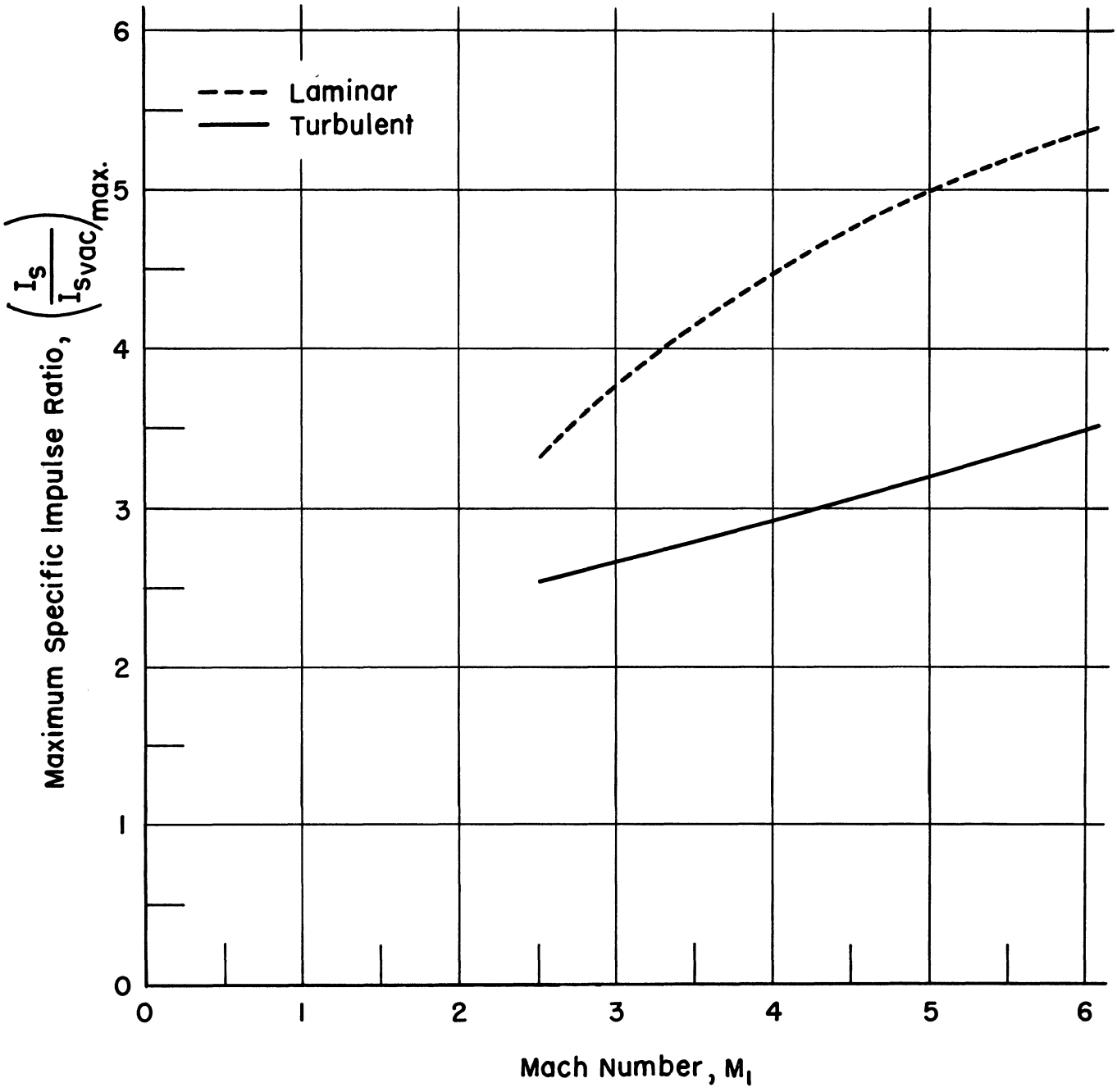

Fig. 8. Variation of maximum value of specific impulse ratio with Mach number. Re_L = 500,000, w^*/L = .001, p_b/p_2 = 0, sonic jet.

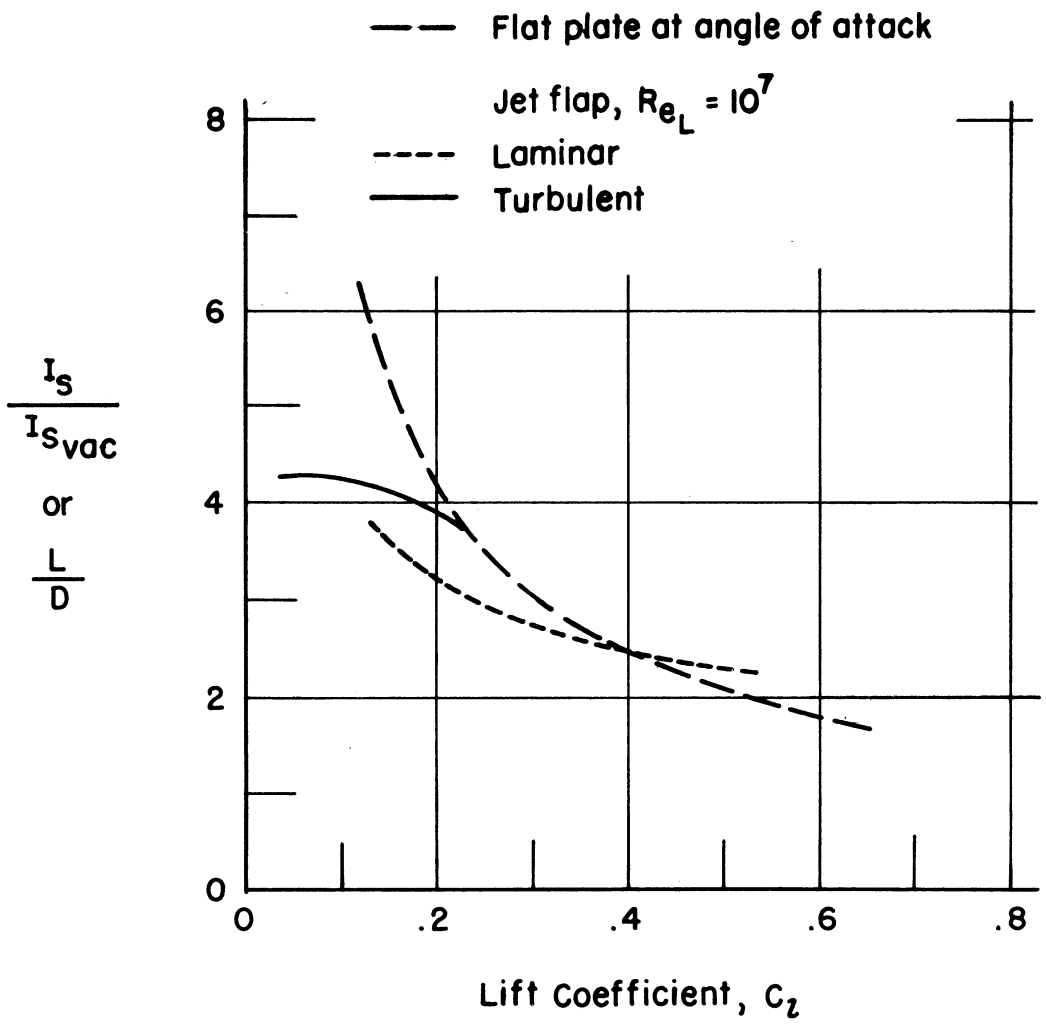

Fig. 9. Lifting efficiency of a two-dimensional jet-flap wing and of a two dimensional flat-plate wing at angle of attack. Skin friction neglected. $M_1 = 6.0$.

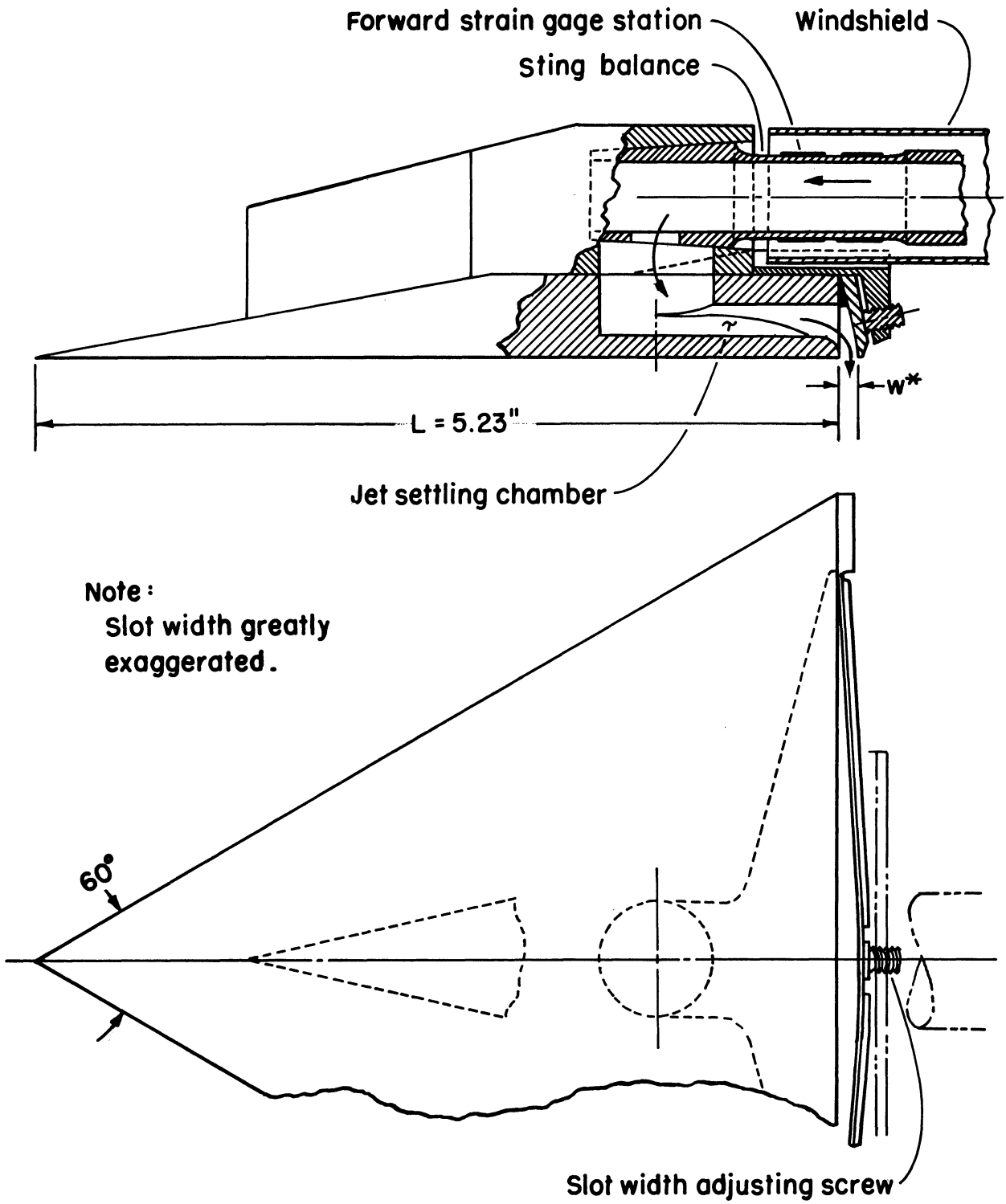

Fig. 10. Tapered jet-flap model.

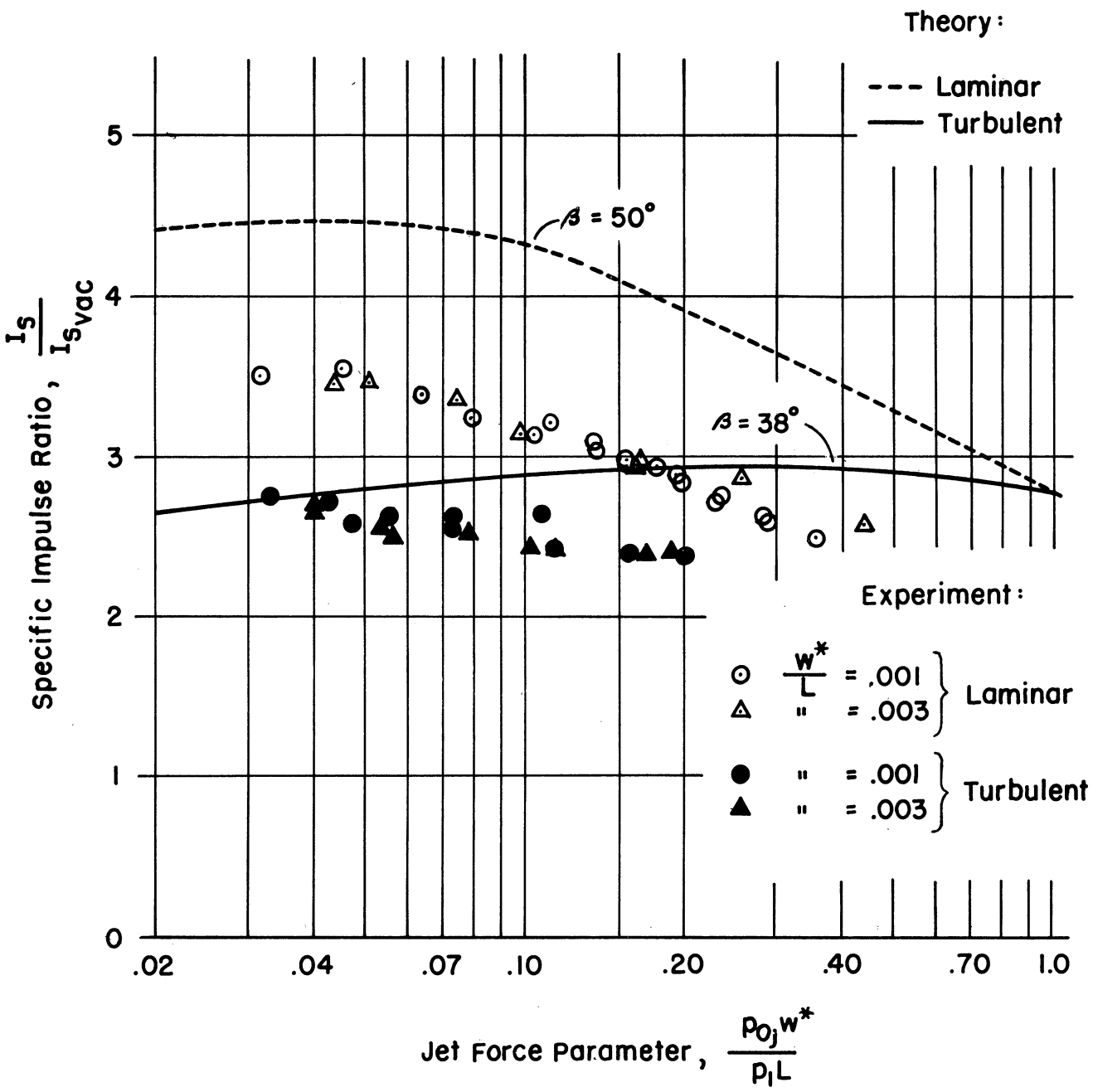

Fig. 11. Specific impulse magnification due to interaction of tapered jet flap on 60° delta wing.

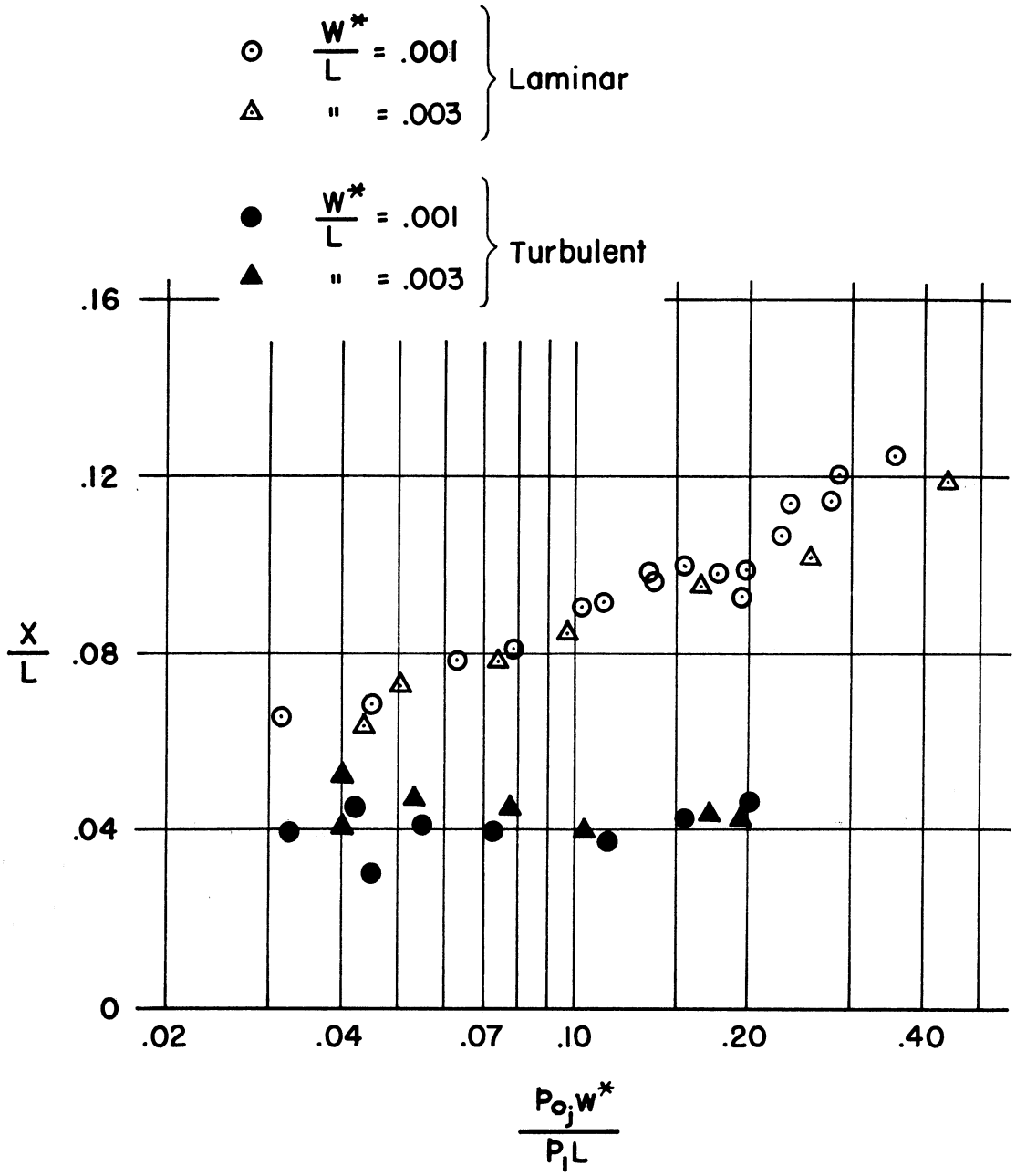

Fig. 12. Distance ahead of slot of line of action of increment in normal force due to tapered jet flap.

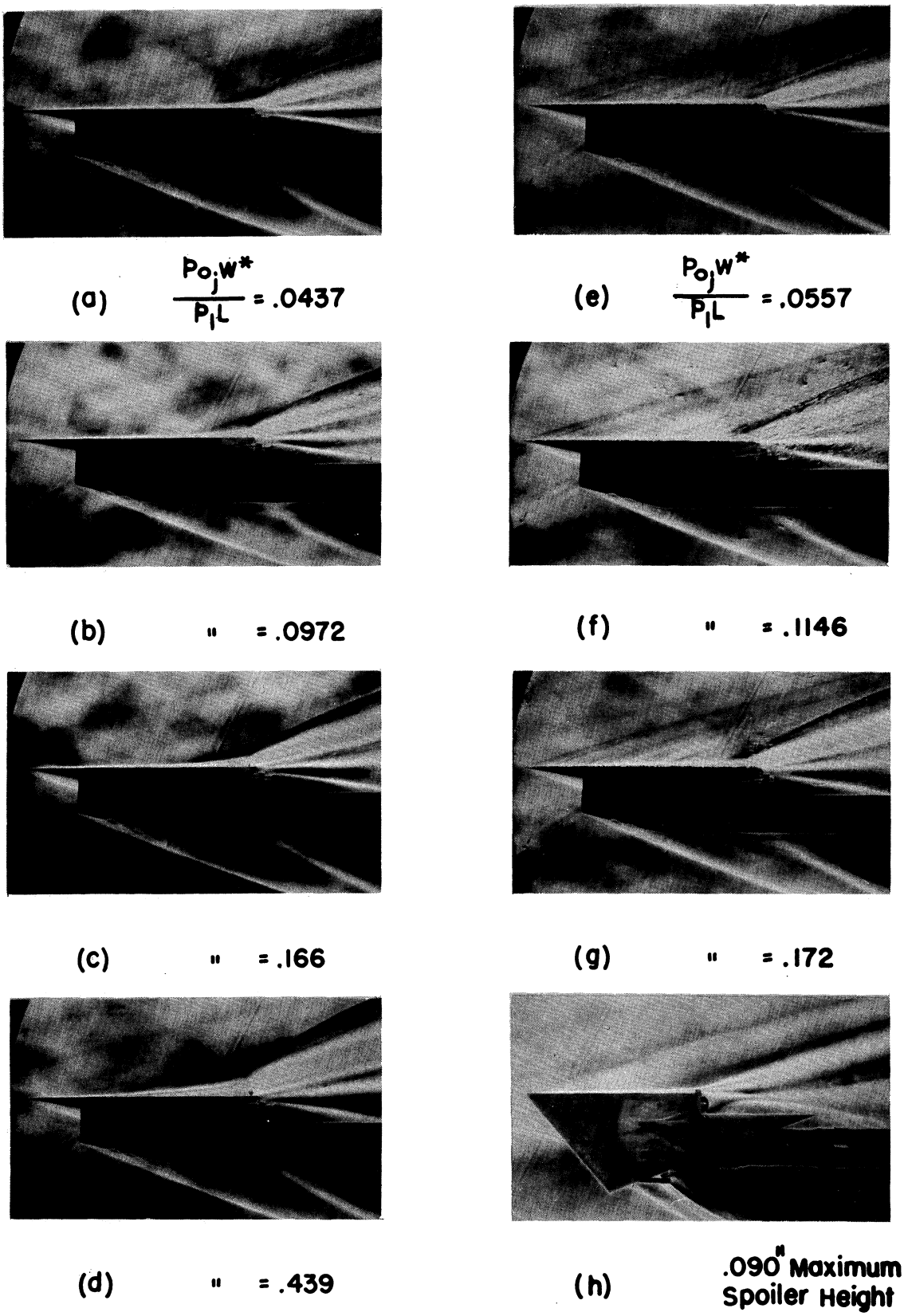

Fig. 13. Typical schlieren pictures of tapered jet-flap interaction.